THE ASTRONOMICAL JOURNAL, 115:418–435, 1998 February

SEEKING THE LOCAL CONVERGENCE DEPTH. II. TULLY-FISHER OBSERVATIONS OF THE CLUSTERS A114, A119, A194, A2295, A2457, A2806, A3193, A3381, AND A3744

DANIEL A. DALE,[1,2] RICCARDO GIOVANELLI,[1,2] MARTHA P. HAYNES,[1] AND MARCO SCODEGGIO[1,3]
Center for Radiophysics and Space Research and National Astronomy and Ionosphere Center, Cornell University, Ithaca, NY 14853;
dale@astrosun.tn.cornell.edu, riccardo@astrosun.tn.cornell.edu, haynes@astrosun.tn.cornell.edu,
scodeggi@astrosun.tn.cornell.edu

EDUARDO HARDY[2]
Département de Physique, Université Laval, Sainte-Foy, QC G1K 7P4, Canada; hardy@phy.ulaval.ca

AND

LUIS E. CAMPUSANO[2]
Observatorio Astronómico Cerro Calán, Departamento de Astronomía, Universidad de Chile, Casilla 36-D, Santiago, Chile;
lcampusa@das.uchile.cl
Received 1997 September 19; revised 1997 November 4

ABSTRACT

We present Tully-Fisher (T-F) observations for nine rich Abell clusters of galaxies. This is the second such data installment of an all-sky survey of ~ 50 clusters in the redshift range $0.02 \lesssim z \lesssim 0.06$. The data extend the T-F study of nearby clusters of Giovanelli et al.; they will be used jointly to determine an accurate I-band T-F template and to establish a cluster inertial reference frame to $z \sim 0.06$.

Key words: cosmology: observations — distance scale — galaxies: distances and redshifts

1. INTRODUCTION

The accurate measurement of deviations from smooth Hubble flow remains a challenge in observational cosmology. The lack of a proven redshift-independent distance estimator applicable beyond $\sim 100\ h^{-1}$ Mpc becomes sorely obvious when claims of large-amplitude coherent flows on scales larger than this are made (Lauer & Postman 1992, hereafter LP; Courteau et al. 1993). Recent observational efforts at constructing relations useful for peculiar velocity measurements (e.g., Riess, Press, & Kirshner 1995; Giovanelli et al. 1996) challenge the LP result, though with insufficient certainty. The Tully-Fisher (T-F; Tully & Fisher 1977) sample of Giovanelli et al. (1996) peculiar velocities is based on a template defined by 555 galaxies in 24 clusters (Giovanelli et al. 1997a, 1997b, hereafter G97a, G97b) that reaches only to $cz \sim 9000$ km s^{-1} and is thus unable to probe the entire peculiar velocity field the LP flow encompasses, whereas the Riess et al. sample of Type Ia supernovae is too sparsely populated to adequately characterize the local bulk flow (Watkins & Feldman 1995). The existing samples of peculiar velocities at relatively large distances ($> 100\ h^{-1}$) need to be enlarged.

We are expanding upon the data of G97a and G97b by obtaining T-F measurements for an all-sky survey of some 50 clusters in the redshift range 5000 km s$^{-1} \lesssim cz \lesssim$ 20,000 km s^{-1}. The benefits of such an enterprise are twofold. First, the combination of our data set with that of G97a and G97b will yield a highly accurate T-F template. The proximity of the extant G97a/G97b sample allows a wide range of galactic properties to be observed and is thus ideal for determining the slope of the T-F relation. On the other hand, the redshifts of our sample of relatively distant clusters are less affected by the vagaries of cosmic peculiar motions, a property useful for accurately extracting the T-F magnitude offset. Second, the combined data set will cover a much larger volume than that of G97a and G97b. Recent work by Scaramella, Vettolani, & Zamorani (1994), Tini-Brunozzi et al. (1995), and Branchini, Plionis, & Sciama (1996) suggests that coherent peculiar motions may persist as far as 18,000 km s^{-1}, i.e., the local "convergence depth" may extend to $\sim 180\ h^{-1}$ Mpc. It thus appears crucial to penetrate the local velocity field as deeply as possible; our sample extends out to and possibly beyond the local convergence depth. This will enable dipole motion measurements over scales large enough to test the claim of LP, whose sample has an effective depth of $\sim 100\ h^{-1}$.

In order to provide public access to the data on the shortest possible timescale, we are presenting results of our survey in installments, as we progress in the data reductions for sizable fractions of the cluster set. Dale et al. (1997, hereafter Paper I) presented T-F measurements for 84 galaxies in the fields of seven Abell clusters. In this paper, we present the project's second data installment: T-F measurements for 90 galaxies in the fields of nine Abell clusters, one of which, the field of A2295, contains two separate clusters (see § 3). The following section reviews the imaging and spectroscopic observations for this data installment. Section 3 presents the relevant T-F data.

2. OBSERVATIONS

Imaging for this project began in 1994 October and is now complete, whereas spectroscopic measurements began in 1995 December and are still ongoing. In the 50 clusters that we have chosen to include in our all-sky survey, we plan to obtain five to 15 T-F measurements per cluster. Including approximately two dozen 21 cm line widths taken earlier by R. G. and M. P. H., we have thus far obtained ~ 360 (cluster member) velocity widths in 48 Abell clusters; we expect to measure ~ 100 more velocity widths. Paper III of this series will present the final installment of data, for the remaining clusters.

[1] Visiting Astronomer, Kitt Peak National Observatory, National Optical Astronomy Observatories (NOAO), operated by the Association of Universities for Research in Astronomy, Inc., under cooperative agreement with the National Science Foundation.

[2] Visiting Astronomer, Cerro Tololo Inter-American Observatory, NOAO.

[3] Current address: European Southern Observatory, Karl-Schwarzschild-Strasse 2, D-85748 Garching bei München, Germany.

TABLE 1

CLUSTER COORDINATES

Cluster (1)	R.A. (B1950.0) (2)	Decl. (B1950.0) (3)	$V_\odot$ (km s^{-1}) (4)	V_{CMB} (km s^{-1}) (5)	N_z (6)	SGL (deg) (7)	SGB (deg) (8)	X (km s^{-1}) (9)	Y (km s^{-1}) (10)	Z (km s^{-1}) (11)
A2806	00 37 54	−56 26 00	8062 (92)	7910	23	240.9	−11.0	−3774	−6787	−1505
A114.....	00 51 12	−21 57 00	17436 (143)	17144	41	275.4	−5.4	1615	−16990	−1624
A119.....	00 53 48	−01 32 00	13377 (153)	13048	37	295.3	−0.7	5581	−11793	−151
A194.....	01 23 00	−01 46 00	5300 (43)	4995	100	−62.9	−7.8	2252	−4407	−674
A3193	03 56 54	−52 29 00	10390 (102)	10354	25	239.9	−39.5	−4001	−6916	−6585
A3381	06 08 06	−33 35 00	11451 (49)	11551	37	234.0	−69.4	−2383	−3287	−10814
A2295B.....	17 59 00	69 16 00	18701 (82)	18633	6	32.5	35.7	12753	8139	10877
A2295	18 00 18	69 13 00	24623 (199)	24555	9	32.4	35.8	16858	10710	14402
A3744	21 04 18	−25 41 00	11692 (61)	11429	57	244.9	37.7	−3828	−8189	6993
A2457	22 33 12	01 13 00	17712 (119)	17349	14	287.5	33.8	4327	−13751	9653

NOTE.—Units of right ascension are hours, minutes, and seconds, and units of declination are degrees, arcminutes, and arcseconds.

2.1. *I-Band Imaging*

All photometric observations were carried out in the I band (Kron-Cousins filter, central wavelength of 8075 Å and passband of 1500 Å), matching those in Paper I, G97a, and G97b. The imaging for the clusters in this paper was carried out at the Kitt Peak National Observatory (KPNO) and Cerro Tololo Inter-American Observatory (CTIO) 0.9 m telescopes. Exposures for each frame amounted to 600 s, a time sufficient to reliably reach isophotal levels near 24.5 mag arcsec^{-2}. The clusters A119, A194, A2295, and A2457 were observed at KPNO over the course of several observing runs: 1994 October 5–16, 1995 September 14–21, 1995 September 21–October 1, 1995 November 20–26, 1996 October 31–November 12, and 1997 February 4–19. The clusters A2806, A114, A3193, A3381, and A3744 were observed at CTIO during the runs of 1995 February 1–8 and 1995 August 28–September 4. We used the same observational methods and technical setups described in Paper I for the KPNO observations; the only significant difference between imaging at KPNO and CTIO for our cluster sample is the higher spatial resolution for the data taken at the CTIO 0.9 m telescope (0.″4 pixel^{-1} vs. 0.″68 pixel^{-1}), and a smaller field of view (14′ × 14′ vs. 23′ × 23′) for the 2048^2 pixel CCD. The average FWHM seeing for the images used in this data set was 1.″7 ± 0.″2 at KPNO and 1.″4 ± 0.″2 at CTIO; however, the nights with the best seeing conditions were preferentially devoted to the more distant clusters. The majority of the data presented here were taken in good photometric conditions, for which the photometric zero-point calibration could be determined with an accuracy of 0.02 mag or better. In a minority of cases (2%), photometric conditions were of inferior quality. In those cases, frames were taken with a substantial sky overlap with images taken in good photometric conditions, so that fluxes of at least 12 field stars could be measured in the overlap region, thus guaranteeing calibration to the ∼0.03 mag level.

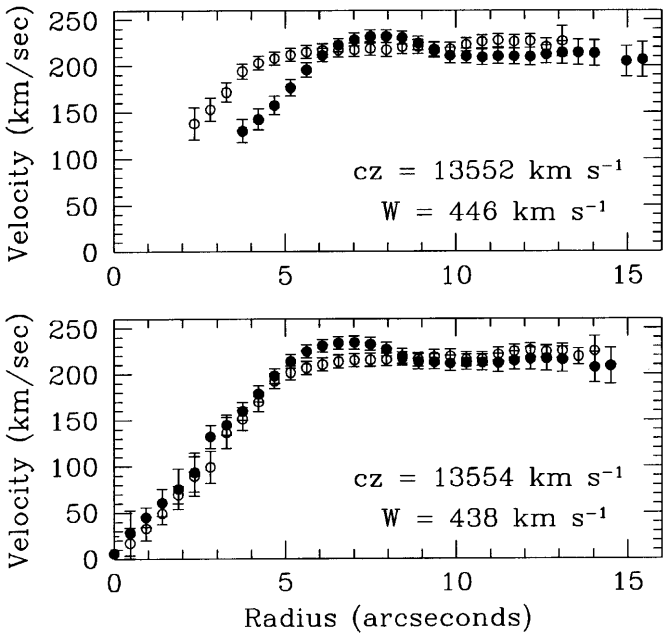

FIG. 1.—Effect of an [N II] data patch on a kinematically folded Hα rotation curve lacking data in the central regions because of absorption. The top panel displays the Hα rotation curve for galaxy 400641 in Abell 119 without the patch, and the bottom panel includes the [N II] data patch. Note that the kinematic recentering changes the definition of the ORC's origin in the spatial direction as well as in the velocity direction.

The determination of I-band fluxes follows from data reduction methods discussed in Paper I and Haynes et al. (1998), using both standard and customized IRAF[4] packages. We will only mention here that the measured fluxes, denoted m_∞, include extrapolations of the exponential fits to the surface brightness profiles to infinity and are typically accurate to ∼0.03 mag (uncertainties at least this large are included later, after corrections for internal extinction are made; see Paper I for details on flux errors). We apply several corrections to m_∞, to obtain

$$m_{\rm cor} = m_\infty - A_I + k_I - \Delta m_{\rm int} - \Delta m_T \,. \quad (1)$$

The first correction, A_I, is for the extinction caused by the Milky Way. We use Burstein & Heiles's (1978) tabulation of Galactic extinction values by averaging entries in the Third Reference Catalogue of Bright Galaxies (RC3; de Vaucouleurs et al. 1991) found near the cluster centers. We convert B-band results to I-band via $A_I = 0.45A_B$; values of A_I for the nine clusters presented here range from 0.00 to 0.17 mag. The internal extinction correction, $\Delta m_{\rm int}$, is applied using the procedure outlined in G97a,

$$\Delta m_{\rm int} = -f(T)\gamma(W_{\rm cor}) \log (1 - e) \,, \quad (2)$$

where γ ($\lesssim$1.0) depends on the corrected velocity width $W_{\rm cor}$ (§ 2.2) and e is the ellipticity of the spiral disk, corrected for

[4] IRAF, the Image Reduction and Analysis Facility, is distributed by NOAO.

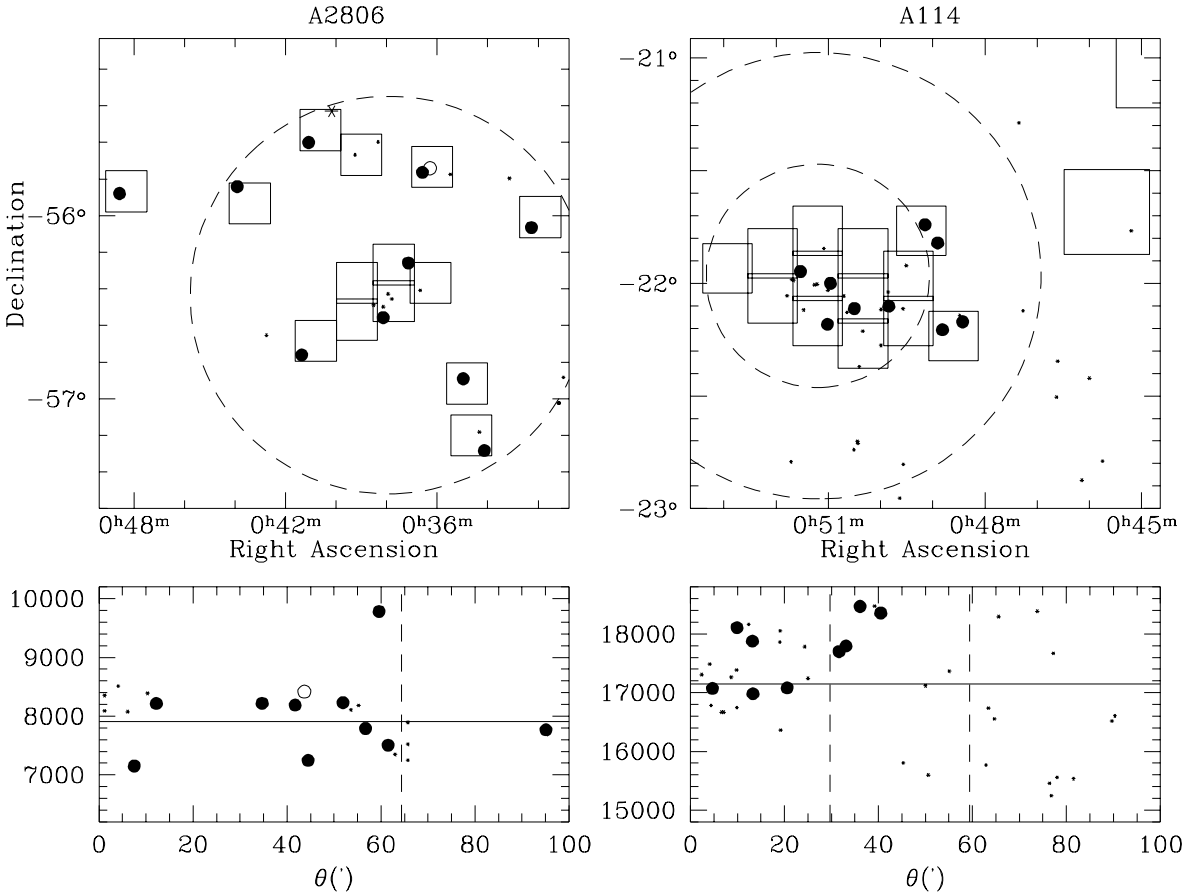

FIG. 2.—Sky and velocity distribution of galaxies in the clusters Abell 2806 and Abell 114. Circles represent cluster members with measured photometry and widths; if unfilled, the widths are poorly determined. Asterisks identify foreground and background galaxies, and dots show the location of galaxies with known redshift but lacking accurate width and/or photometry. Squares indicate outlines of imaged fields with the 0.9 m telescope. Vertical dashed lines in the bottom panels indicate $1R_A$ (and $2R_A$ for A114). The top panels contain circles of radius $1R_A$ (and $2R_A$ for A114).

atmospheric seeing effects as described in § 5 of Paper I [the adopted correction $\Delta m_{\rm int}$ is slightly smaller for early, less dusty galaxies: $f(T) = 0.85$ for types T earlier than Sbc, $f(T) = 1$ otherwise]. We apply a cosmological k-correction $k_I = (0.5876 - 0.1658T)z$ (Han 1992). Finally, we include a small correction, Δm_T, for the T-F dependence on morphological type found in G97b; while the true, unextincted, face-on apparent magnitude of the galaxy is $m_{\rm cor} + \Delta m_T$, $m_{\rm cor}$ represents the value to be used in T-F work with the template T-F relation obtained in G97b, characterized for Sbc and Sc galaxies. Thus $\Delta m_T = 0$ for types Sbc and later; the correction is 0.1 mag for Sb types and 0.32 mag for types earlier than Sb.

2.2. *Optical Spectroscopy*

Rotational velocity widths for this sample of cluster galaxies were extracted from long-slit spectra obtained at the Palomar Observatory 5 m telescope and the CTIO 4 m telescope. The clusters A114, A119, A194, A2295, A3744, and A2457 were observed at Palomar during the runs of 1995 October 22–23, 1995 December 13–18, 1996 July 9–12, and 1996 September 13–19. The clusters A2806, A3193, and A3381 were observed at CTIO during the nights of 1996 April 4–7 and 1996 September 30–October 3. We refer the reader to Paper I for details of the spectroscopy performed at Palomar. The observing setup at the CTIO 4 m uses the Ritchey-Chrétien spectrograph and the Loral 3072 × 1024 pixel CCD with a 203″ long slit. The combination of the 1200 line $\rm mm^{-1}$ grating and a 2″ wide slit yields a dispersion of 0.55 Å $\rm pixel^{-1}$ and a spectral resolution of 1.7 Å (equivalent to 75 km $\rm s^{-1}$ at 6800 Å). Along the cross-dispersion axis, the spatial scale is 0.″50 $\rm pixel^{-1}$. The wavelength range (∼5640–7320 Å) is large enough to observe redshifted Hα emission in galaxies with recessional velocities up to ∼34,000 km $\rm s^{-1}$ in our chosen setup.

The adopted observing strategy includes a 5 minute preliminary integration on each galaxy. This allows a quick estimate of the spectral lines' strength, from which we determine the exposure time necessary to adequately sample the outer disk regions. Moreover, performing a 5 minute test exposure informs us if the galaxy is at the cluster redshift and if the distribution of H II regions is sufficient to provide a useful rotation curve. If the observation is deemed useful, a second integration of usually 15–45 minutes is taken.

We extract optical rotation curves (ORCs) as discussed in Paper I. We used the Hα (6563 Å) emission line to map out the ORC except in 2% of the cases, in which the emission of the [N II] 6584 Å line extends to larger radii than that of the Hα emission. We kinematically center the ORC by assigning the velocity nearest the average of the 10% and 90% velocities to be at radius zero, where an N% velocity is such that N% of the data points in the rotation curve have velocity smaller than it. The average of the 10% and 90% velocities is taken to be the galaxy's recessional velocity. We

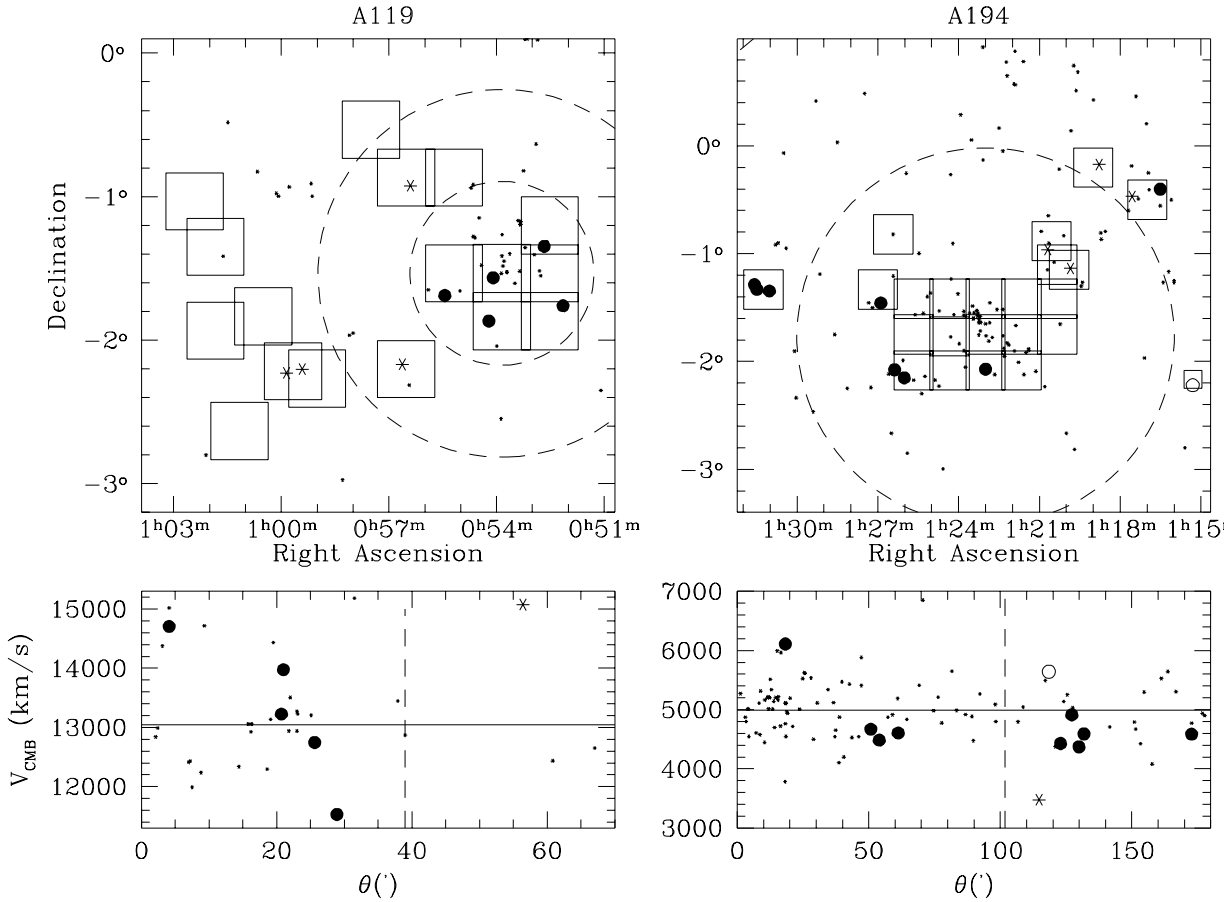

FIG. 3.—Same as Fig. 2, but for the clusters Abell 119 and Abell 194

define the observed rotational velocity width to be $W_{obs} \equiv V_{90\%} - V_{10\%}$. In regions where heavy Hα absorption and emission are mixed, usually near the galactic center, we fill in the portions of the rotation curve with data from the [N II] rotation curve, if available. We do this to provide information on the shape of the inner portions of all ORCs and to ensure that our method of computing W_{obs} does not artificially yield slightly large values when data are missing. We applied this [N II] patch to approximately 10% of the Hα ORCs; the notes on individual galaxies in § 3 indicate which ORCs include [N II] patches. In Figure 1, we display the effect that an [N II] patch can have on an ORC, using the ORC of galaxy 400641 in A119 as an example. The top panel shows the Hα ORC without the [N II] patch, and the bottom panel includes the patch. The effect on the inferred redshift and W_{obs} is small, but the shape of the ORC has changed significantly. This change is in part due to the kinematic recentering of the ORC—the origin of the ORC has also been shifted radially (by 0.″94). If information on the central portions of an ORC is lacking for all spectral lines available, we consider the peak of the galactic continuum light profile, formed by summing the data along the dispersion direction, to represent the spatial center of the galaxy (see, e.g., Fig. 1, *top*).

The method described above for characterizing rotational velocity widths is used since it effectively ignores small-scale velocity irregularities within an ORC that may arise from streaming motions within the galactic disk, the non-uniform distribution of H II regions, or distortions associated with the spiral pattern. Furthermore, we find empirically that, provided the rotation curve extends far enough out into the disk, this method recovers the velocity width at R_{opt}, the distance along the major axis to the isophote containing 83% of the *I*-band flux. This is reported by Persic & Salucci (1991, 1995) to be a useful radius at which to measure the velocity widths of ORCs. Thus, extrapolations to the ORC, and hence adjustments to W_{obs}, are made in cases in which the ORC's radial extent falls well short of R_{opt}. The resulting correction, which depends on the shape of the rotation curve, Δ_{sh}, rarely exceeds $0.1W_{obs}$.

To recover the actual velocity widths, two more corrections are necessary. The first is the factor $1/\sin i$ necessary to convert the width observed for a disk inclined to the line of sight at an angle i to what would be observed if the disk were edge-on, and the second is the factor $1/(1+z)$ to correct for the cosmological broadening of W. The corrected optical rotational velocity width is then

$$W_{cor} = \frac{W_{obs} + \Delta_{sh}}{(1+z)\sin i}. \quad (3)$$

A discussion of the errors in the velocity widths can be found in Paper I.

In addition to the 82 ORCs presented here, we also have 21 cm measurements for eight galaxies, all members of A194. Six of the eight H I spectra were taken at the Arecibo Observatory using a spectrometer channel separation of 8 km s^{-1}, while the remaining two were obtained at the Green Bank 300 foot (91 m) telescope (Haynes & Giovanelli 1991) at a spectral resolution of 11 km s^{-1}. A typical signal-

TABLE 2

GALAXY SPECTROSCOPIC PARAMETERS BY CLUSTER

Galaxy (1)	R.A. (B1950.0) (2)	Decl. (B1950.0) (3)	$V_{\odot}$ (km s^{-1}) (4)	$V_{\rm CMB}$ (km s^{-1}) (5)	$W_{\rm obs}$ (km s^{-1}) (6)	W (km s^{-1}) (7)	$W_{\rm cor}$ (km s^{-1}) (8)	i (deg) (9)	log $W_{\rm cor}$ (10)	Notes (11)
A2806:										
20391	00 32 16.2	−56 03 54	8387 (13)	8231	494	502	516	77	2.713 (18)	a
400697.....	00 34 07.7	−57 17 00	9928 (10)	9779	293	284	286	83	2.456 (28)	
400698.....	00 34 58.0	−56 53 27	7400 (08)	7249	242	265	278	72	2.444 (35)	a
400703.....	00 36 16.6	−55 44 27	8574 (12)	8417	208	218	279	51	2.446 (63)	a
400704.....	00 36 35.1	−55 45 48	8344 (08)	8188	172	167	200	57	2.301 (32)	
400706.....	00 37 08.4	−56 15 31	8370 (07)	8216	229	223	227	79	2.356 (23)	
400713.....	00 38 08.0	−56 33 16	7304 (07)	7152	196	221	241	66	2.382 (44)	a
20487	00 41 05.0	−55 36 01	7948 (07)	7792	406	396	414	73	2.617 (16)	
400727.....	00 41 21.6	−56 45 38	8369 (07)	8219	248	241	248	77	2.394 (26)	
20512	00 43 54.4	−55 50 28	7660 (07)	7506	414	404	413	78	2.616 (17)	
20587	00 48 34.3	−55 52 44	7919 (07)	7767	425	414	421	80	2.624 (17)	
A114:										
400421.....	00 48 25.6	−22 10 15	18649 (07)	18356	546	514	527	78	2.722 (11)	
400672.....	00 48 48.8	−22 12 22	18760 (07)	18467	289	272	284	74	2.453 (15)	a
400673.....	00 48 54.3	−21 49 15	18092 (07)	17798	272	270	287	70	2.458 (25)	
400674.....	00 49 08.9	−21 44 23	17989 (08)	17695	196	195	196	84	2.291 (32)	
400443.....	00 49 50.5	−22 06 06	17373 (07)	17081	356	337	427	52	2.630 (54)	a
400453.....	00 50 28.2	−22 06 44	17274 (07)	16982	377	357	387	67	2.588 (14)	a
400686.....	00 50 57.6	−22 07 16	18401 (07)	18109	409	386	400	75	2.602 (14)	
400466.....	00 51 00.9	−22 10 55	18169 (07)	17878	448	423	453	69	2.656 (13)	
400688.....	00 51 32.0	−21 56 52	17364 (07)	17072	344	325	347	70	2.540 (19)	
A119:										
400611.....	00 52 08.8	−01 45 37	11860 (08)	11530	508	489	507	75	2.705 (16)	
400619.....	00 52 40.2	−01 20 48	14306 (07)	13976	391	374	382	78	2.582 (17)	a
400600.....	00 54 05.6	−01 33 55	15036 (10)	14707	367	363	377	75	2.576 (22)	a
400641.....	00 54 13.3	−01 52 01	13554 (08)	13226	438	419	462	65	2.665 (21)	a
400653.....	00 55 26.5	−01 41 21	13073 (07)	12745	286	274	278	81	2.444 (17)	
400658.....	00 56 23.9	−00 55 31	22779 (07)	22451	414	385	416	68	2.619 (14)	a
A194:										
784.....	01 11 31.1	−02 00 22	4901 (05)	4586	299[b]	268	299	64	2.476 (22)	a
830.....	01 15 18.4	−02 13 12	5954 (06)	5642	109[b]	90	154	36	2.188 (67)	a
847.....	01 16 30.8	−00 24 05	5218 (08)	4905	249	254	254	90	2.405 (29)	
894.....	01 18 47.4	−00 10 15	3790 (07)	3479	192[b]	166	178	69	2.250 (35)	a
915.....	01 19 50.5	−01 08 08	8145 (04)	7836	561[b]	516	560	67	2.748 (15)	a
931.....	01 20 41.2	−00 57 41	2001 (04)	1692	121[b]	103	105	78	2.023 (56)	a
410188.....	01 23 00.2	−02 04 18	6416 (07)	6111	155	160	181	62	2.259 (34)	
410583.....	01 26 01.2	−02 09 05	4978 (07)	4675	184	181	189	74	2.276 (38)	
1060	01 26 22.8	−02 04 39	4787 (07)	4484	233	230	240	73	2.380 (22)	
410584.....	01 26 53.3	−01 27 28	4909 (07)	4606	248	244	249	79	2.397 (23)	a
1116	01 31 01.5	−01 20 47	4720 (25)	4421	284[b]	259	263	80	2.420 (75)	a
1120	01 31 29.3	−01 19 53	4664 (08)	4365	371[b]	340	346	79	2.539 (20)	a
1123	01 31 34.8	−01 17 15	4916 (20)	4618	448[b]	430	432	84	2.636 (40)	a
A3193:										
430691.....	03 55 36.4	−52 32 41	10148 (07)	10111	264	255	282	65	2.450 (31)	
430695.....	03 56 38.0	−52 23 50	9720 (10)	9683	216	213	251	58	2.399 (35)	
430697.....	03 57 04.9	−52 16 55	10299 (07)	10262	394	381	393	76	2.594 (21)	
430698.....	03 57 37.0	−52 41 45	10458 (07)	10423	177	181	187	76	2.271 (29)	
23113	03 58 22.6	−52 49 16	9796 (07)	9762	212	205	327	39	2.515 (78)	a
23130	03 59 23.4	−52 52 22	10569 (07)	10536	255	257	308	56	2.489 (42)	a
23136	04 00 00.5	−52 50 44	9965 (07)	9932	391	378	519	47	2.715 (27)	a
A3381:										
460069.....	06 07 40.0	−33 37 01	11199 (07)	11298	378	389	404	75	2.606 (35)	a
460070.....	06 07 40.7	−33 32 30	10309 (08)	10408	307	297	308	75	2.488 (26)	
460071.....	06 07 49.2	−33 34 35	11149 (07)	11249	285	285	315	65	2.498 (36)	a
460077.....	06 08 32.3	−33 40 45	9004 (07)	9105	287	279	334	57	2.523 (25)	
24895	06 09 15.8	−33 17 18	11517 (07)	11619	342	330	347	72	2.540 (33)	a
A2295B:										
270368.....	17 56 13.4	69 03 21	18844 (07)	18778	274	258	289	63	2.461 (31)	
270370.....	17 56 36.9	69 03 15	18835 (10)	18769	277	297	298	88	2.474 (39)	a
280128.....	18 01 21.3	69 29 35	18535 (07)	18466	385	367	378	76	2.578 (23)	a
280130.....	18 02 09.7	69 30 46	18482 (07)	18413	474	447	537	56	2.730 (28)	a
280134.....	18 04 10.5	69 22 40	15740 (07)	15670	433	411	418	80	2.621 (15)	a
A2295:										
270373.....	17 58 23.3	69 04 35	25332 (07)	25265	322	297	340	61	2.532 (20)	
270375.....	17 58 26.1	69 17 38	24430 (07)	24363	270	277	473	36	2.675 (58)	a
270378.....	17 59 10.3	69 05 45	24513 (07)	24445	353	350	351	84	2.546 (24)	
270379.....	17 59 20.9	69 01 46	24410 (07)	24342	328	303	326	69	2.513 (15)	
280122.....	18 00 06.7	69 11 27	23744 (10)	23676	456	423	436	76	2.640 (16)	
280126.....	18 01 08.3	69 19 26	25236 (07)	25167	476	439	485	65	2.686 (13)	
280131.....	18 02 10.3	68 42 36	27425 (07)	27355	560	513	518	83	2.714 (11)	a

TABLE 2—*Continued*

Galaxy (1)	R.A. (B1950.0) (2)	Decl. (B1950.0) (3)	$V_\odot$ (km s^{-1}) (4)	V_{CMB} (km s^{-1}) (5)	W_{obs} (km s^{-1}) (6)	W (km s^{-1}) (7)	W_{cor} (km s^{-1}) (8)	i (deg) (9)	log W_{cor} (10)	Notes (11)
280132.....	18 02 11.5	69 14 30	25391 (07)	25322	335	309	329	70	2.517 (16)	
280133.....	18 03 35.0	69 16 51	24728 (07)	24658	434	404	432	69	2.636 (23)	
280136.....	18 04 46.6	69 15 21	27367 (07)	27296	370	339	362	70	2.558 (16)	a
A3744:										
610196.....	21 02 24.6	−25 46 03	11234 (07)	10972	171	230	232	82	2.365 (65)	a
610198.....	21 02 43.2	−25 45 05	12171 (07)	11909	128	144	146	82	2.163 (41)	a
34131	21 03 28.5	−24 33 58	11077 (07)	10811	186	186	206	65	2.314 (69)	a
34135	21 03 31.0	−24 36 49	11160 (09)	10894	365	382	414	68	2.617 (28)	
610212.....	21 03 36.2	−24 41 22	10394 (07)	10128	194	201	202	87	2.304 (34)	
610214.....	21 03 44.2	−25 40 01	11298 (07)	11035	295	285	285	88	2.454 (25)	
610217.....	21 04 05.5	−24 49 17	11312 (07)	11046	234	226	232	76	2.366 (28)	
610220.....	21 04 15.7	−25 27 16	11602 (10)	11338	307	296	329	64	2.517 (29)	a
610222.....	21 04 25.0	−25 49 55	12204 (07)	11941	383	381	384	83	2.584 (24)	a
610224.....	21 04 27.7	−25 46 23	12740 (07)	12477	201	206	214	75	2.331 (30)	
610231.....	21 04 44.0	−24 51 30	11145 (08)	10879	378	365	415	61	2.619 (22)	
34189	21 06 11.4	−25 45 32	8793 (09)	8529	224	218	221	80	2.345 (45)	a
610251.....	21 06 20.6	−25 45 50	8876 (07)	8611	153	153	153	85	2.185 (42)	a
A2457:										
320569.....	22 31 29.7	01 39 29	18084 (07)	17721	551	520	535	77	2.728 (12)	
320572.....	22 31 57.3	01 18 08	18281 (08)	17918	433	452	454	85	2.657 (33)	a
320573.....	22 31 59.2	01 09 26	17815 (07)	17452	343	329	357	67	2.552 (25)	a
320574.....	22 32 03.8	01 40 07	20992 (08)	20629	399	373	377	82	2.577 (16)	a
320575.....	22 32 10.5	01 06 02	17779 (07)	17416	500	473	475	84	2.677 (17)	
320576.....	22 32 36.9	01 05 14	18254 (07)	17891	417	394	495	53	2.695 (53)	a
320578.....	22 32 37.2	00 35 15	17786 (08)	17424	398	376	377	87	2.576 (16)	
320579.....	22 33 01.0	01 36 03	16777 (07)	16414	281	276	310	63	2.492 (32)	a
320581.....	22 33 08.8	01 24 01	16933 (07)	16570	531	503	560	64	2.748 (15)	a
320583.....	22 33 33.7	01 17 59	16023 (07)	15660	358	340	351	76	2.545 (22)	a
320591.....	22 34 17.2	01 22 19	11300 (08)	10937	380	367	367	86	2.565 (18)	a

NOTE.—Units of right ascension are hours, minutes, and seconds, and units of declination are degrees, arcminutes, and arcseconds.

[a] See § 3 for notes on individual galaxies.

[b] Line width from 21 cm data.

to-noise ratio for these observations was 10; errors in the observed velocity widths are of order 15 km s^{-1}. Details on the H I data reduction and the corrections made to the observed velocity widths can be found in G97a. A full discussion of the comparison between H I and optical widths is given in Giovanelli et al. (1998).

3. DATA

Table 1 lists the main parameters of the clusters. Standard names are listed in column (1). Adopted coordinates of the cluster center are listed in columns (2) and (3), for epoch B1950.0; they were obtained from Abell, Corwin, & Olowin (1989) except for the entry A2295B, a system found to be slightly offset from A2295 in both sky position and redshift. For all of the clusters, we derived a new systemic velocity, combining the redshift measurements available in the NED[5] database with our own. These newly determined velocities are listed in columns (4) and (5), in the heliocentric and in the cosmic microwave background (CMB) reference frames (Kogut et al. 1993), respectively. We list the number of cluster member redshifts used in determining systemic velocities in column (6). An estimated error for the systemic velocity is parenthesized after the heliocentric figure. Spherical and Cartesian supergalactic coordinates are given in columns (7) and (8) and in columns (9)–(11), respectively.

Figures 2–6 show the distribution of the galaxies in each cluster. The top panels in each of these figures display the spatial location of the outline of the fields imaged (*squares*), cluster members (*circles*; those with poor/unusable velocity widths are left unfilled), background or foreground objects (*asterisks*), and galaxies with known redshift but without reliable widths (*dots*). Circles of 1 and 2 Abell radii, R_A, are drawn as dashed lines if the area displayed is large enough. If no dashed circle is drawn, R_A is larger than the figure limits. We also plot radial (CMB) velocity as a function of angular distance from the cluster center in the bottom panels of each figure. A dashed vertical line is drawn at $1R_A$. The combination of the sky and velocity plots is used to gauge cluster membership for each galaxy.

We separate photometric data and spectroscopic data into two tables. Table 2 lists the spectroscopic properties, and Table 3 gives the pertinent photometric results. Entries in the tables are sorted first by the right ascension of each cluster and, within each cluster sample, by increasing galaxy right ascension. The listed parameters for Table 2 are as follows:

Column (*1*).—Identification names corresponding to a coding number in our private database, referred to as the Arecibo General Catalog, which we maintain for easy reference in case readers may request additional information on the object.

Columns (*2*), (*3*).—Right ascension and declination in the B1950.0 epoch. Coordinates have been obtained from the Digitized Sky Survey catalog and are accurate to better than 2″.

Columns (*4*), (*5*).—The galaxy radial velocity as measured in the heliocentric and CMB reference frames (Kogut et al. 1993), respectively. Errors are parenthesized: e.g., 13241 (08)

[5] The NASA/IPAC Extragalactic Database is operated by the Jet Propulsion Laboratory, California Institute of Technology, under contract with the National Aeronautics and Space Administration.

TABLE 3

GALAXY PHOTOMETRIC PARAMETERS BY CLUSTER

Galaxy (1)	T (2)	θ (arcmin) (3)	P.A. (deg) (4)	ϵ (5)	ϵ_{cor} (6)	$\mu(0)$ (7)	R_d (arcsec) (8)	R_{opt} (arcsec) (9)	$R_{23.5}$ (arcsec) (10)	$m_{23.5}$ (11)	m_{∞} (12)	m_{cor} (13)	M_{cor} (14)	Notes (15)
A2806:														
20391	1	52	95	0.681	0.698 (12)	17.9	7.7	27.8	39.5	12.72	12.69	12.10	−22.39 (07)	a
400697.....	5	60	72	0.804	0.823 (13)	19.4	8.4	23.9	32.2	14.55	14.49	13.80	−21.15 (11)	
400698.....	3	37	0	0.602	0.637 (15)	17.2	3.0	11.5	17.5	14.28	14.26	13.81	−20.68 (07)	a
400703.....	5	44	18	0.359	0.367 (26)	19.7	7.2	21.4	25.0	13.94	13.81	13.63	−20.86 (05)	a
400704.....	5	42	143	0.421	0.441 (24)	18.6	3.5	12.1	15.7	14.78	14.69	14.48	−20.01 (05)	
400706.....	5	12	74	0.755	0.776 (19)	20.1	7.5	20.1	23.6	15.26	15.13	14.59	−19.90 (10)	
400713.....	5	8	44	0.561	0.582 (16)	19.1	4.8	15.2	19.9	14.65	14.58	14.27	−20.23 (06)	a
20487	3:	57	5	0.635	0.647 (10)	18.5	10.2	40.0	52.2	12.69	12.63	12.31	−22.18 (06)	
400727.....	5	35	141	0.717	0.744 (08)	19.4	6.4	18.8	24.2	14.91	14.83	14.34	−20.15 (09)	
20512	1:	62	91	0.691	0.713 (25)	18.1	6.3	25.9	36.8	13.16	13.14	12.52	−21.97 (12)	
20587	2	95	158	0.717	0.738 (16)	19.0	8.7	26.2	36.0	13.44	13.38	12.71	−21.75 (12)	
A114:														
400421.....	3	40	120	0.686	0.710 (25)	19.0	5.8	17.6	23.6	14.32	14.26	13.85	−22.47 (11)	
400672.....	5	36	62	0.652	0.690 (21)	19.4	3.4	10.2	12.8	16.01	15.92	15.45	−20.89 (08)	a
400673.....	5	33	104	0.588	0.638 (07)	18.5	2.2	7.4	10.3	15.84	15.80	15.38	−20.87 (07)	
400674.....	5	32	143	0.800	0.836 (14)	20.7	4.7	13.5	12.2	17.49	17.24	16.70	−19.54 (11)	
400443.....	1	21	48	0.341	0.366 (89)	17.5	2.3	8.4	12.8	14.33	14.30	13.84	−22.33 (07)	a
400453.....	4	13	140	0.561	0.594 (22)	18.1	2.7	10.7	13.6	14.75	14.70	14.42	−21.75 (05)	a
400686.....	3:	10	103	0.628	0.675 (16)	18.9	2.8	8.5	11.9	15.73	15.66	15.29	−20.88 (06)	
400466.....	2	13	58	0.567	0.597 (16)	18.7	3.9	11.7	17.2	14.63	14.58	14.03	−22.14 (07)	
400688.....	4:	5	112	0.616	0.632 (07)	19.8	6.3	17.3	21.3	14.82	14.71	14.41	−21.76 (06)	
A119:														
400611.....	2	29	8	0.653	0.674 (20)	19.3	6.8	18.6	26.6	13.99	13.93	13.30	−22.00 (07)	
400619.....	3	21	9	0.690	0.713 (17)	19.0	6.7	18.5	27.4	14.12	14.07	13.60	−21.98 (10)	a
400600.....	3	4	102	0.641	0.673 (15)	18.1	4.3	12.9	21.1	14.09	14.06	13.62	−21.95 (06)	a
400641.....	3:	21	130	0.512	0.542 (53)	18.5	3.9	12.8	18.2	14.35	14.30	13.97	−21.61 (06)	a
400653.....	6	26	91	0.749	0.794 (10)	19.3	4.0	11.9	15.3	16.09	16.02	15.35	−20.23 (10)	
400658.....	5	53	44	0.579	0.604 (22)	20.2	4.3	11.8	14.8	15.48	15.37	15.10	−21.66 (05)	a
A194:														
784.....	3:	173	30	0.507	0.522 (12)	18.9	7.1	22.6	29.3	13.43	13.37	12.95	−20.36 (06)	a
830.....	5	118	120	0.185	0.185 (15)	20.5	13.5	52.4	37.1	13.38	13.09	12.98	−20.78 (08)	a
847.....	5	127	67	0.878	0.893 (13)	20.1	14.6	41.8	46.0	14.72	14.57	13.56	−19.89 (15)	
894.....	5:	115	105	0.598	0.619 (13)	18.0	5.6	22.5	28.2	13.93	13.87	13.52	−19.19 (05)	a
915.....	4	61	132	0.584	0.592 (12)	18.5	14.3	48.5	66.6	11.86	11.80	11.51	−22.96 (04)	a
931.....	5	59	7	0.736	0.753 (09)	20.3	9.8	28.5	28.6	14.99	14.78	14.37	−16.77 (07)	a
410188.....	5	18	4	0.479	0.512 (27)	18.8	3.8	14.7	18.1	14.78	14.70	14.43	−19.07 (05)	
410583.....	5	51	22	0.632	0.692 (14)	18.8	3.0	9.5	13.1	15.71	15.65	15.23	−18.26 (06)	
1060	5	54	82	0.656	0.682 (13)	19.6	7.1	21.1	25.2	14.69	14.58	14.10	−19.39 (07)	
410584.....	4	61	74	0.737	0.764 (13)	19.1	6.0	17.3	24.4	14.53	14.45	13.86	−19.64 (09)	a
1116	5	123	115	0.761	0.786 (31)	18.3	7.2	25.4	34.3	13.77	13.73	13.05	−20.18 (11)	a
1120	2	130	138	0.712	0.730 (10)	18.6	8.9	27.1	40.1	12.96	12.91	12.17	−21.03 (11)	a
1123	1	132	71	0.758	0.777 (08)	17.6	8.8	26.9	46.5	12.40	12.39	11.55	−21.78 (13)	a
A3193:														
430691.....	5	12	9	0.542	0.559 (12)	19.3	5.5	18.8	21.2	14.82	14.69	14.37	−20.70 (07)	
430695.....	5	6	144	0.447	0.461 (27)	20.0	5.2	16.2	16.5	15.38	15.19	14.97	−20.11 (07)	
430697.....	3	12	158	0.658	0.688 (07)	17.4	3.9	14.5	22.5	13.79	13.77	13.39	−21.69 (06)	
430698.....	5	14	57	0.689	0.722 (09)	19.1	3.7	12.3	14.0	16.15	16.04	15.67	−19.41 (07)	
23113	5:	24	39	0.209	0.217 (52)	18.9	3.7	11.3	15.6	14.26	14.19	14.13	−20.95 (04)	a
23130	2:	33	165	0.420	0.423 (40)	21.7	19.3	52.3	31.8	13.95	13.52	13.01	−22.07 (12)	a
23136	2:	36	45	0.293	0.300 (25)	18.6	5.9	18.2	26.8	13.02	12.97	12.56	−22.51 (06)	a
A3381:														
460069.....	2	6	17	0.639	0.671 (09)	19.1	4.6	13.4	20.2	14.36	14.31	13.73	−21.58 (07)	a
460070.....	2	6	108	0.631	0.671 (12)	18.8	3.5	10.2	15.0	15.20	15.15	14.43	−20.88 (09)	
460071.....	2B	4	127	0.524	0.539 (35)	19.8	7.4	20.7	25.2	13.99	13.89	13.28	−22.03 (09)	a
460077.....	4:	8	180	0.420	0.439 (31)	18.4	4.5	14.4	21.0	13.84	13.78	13.61	−21.18 (04)	
24895	4	23	149	0.641	0.672 (15)	18.7	5.7	16.6	24.3	14.20	14.14	13.82	−21.49 (06)	a
A2295B:														
270368.....	5	20	135	0.495	0.534 (54)	19.4	3.3	10.1	12.2	15.60	15.51	15.14	−21.21 (08)	
270370.....	5	18	79	0.806	0.863 (07)	20.0	4.2	13.2	13.8	17.02	16.85	16.00	−20.35 (13)	a
280128.....	4	18	100	0.667	0.732 (17)	18.8	2.8	8.8	12.3	15.85	15.80	15.31	−21.04 (10)	a
280130.....	0	22	96	0.406	0.420 (56)	20.7	7.6	16.9	19.7	14.29	14.15	13.60	−22.75 (07)	a
280134.....	4	28	16	0.728	0.786 (08)	18.8	3.6	10.8	15.5	15.48	15.43	14.80	−21.18 (12)	a
A2295:														
270373.....	3	13	53	0.440	0.482 (28)	19.6	2.7	7.7	9.8	16.01	15.92	15.58	−21.37 (06)	
270375.....	4:	11	63	0.175	0.185 (20)	19.4	3.9	10.2	14.6	14.40	14.32	14.20	−22.75 (04)	a
270378.....	5	9	40	0.765	0.836 (11)	19.1	2.7	9.5	12.2	16.54	16.48	15.71	−21.24 (13)	
270379.....	5	12	45	0.568	0.616 (23)	20.2	2.7	7.4	8.3	16.88	16.75	16.42	−20.53 (06)	
280122.....	4:	2	93	0.664	0.722 (15)	18.8	2.8	9.3	12.3	15.90	15.83	15.40	−21.55 (11)	
280126.....	3	8	59	0.511	0.538 (13)	19.4	4.3	13.0	16.0	15.00	14.91	14.56	−22.39 (06)	
280131.....	1	32	151	0.718	0.763 (10)	18.5	3.8	12.3	17.2	15.24	15.19	14.35	−22.84 (12)	a

TABLE 3—*Continued*

Galaxy (1)	T (2)	θ (arcmin) (3)	P.A. (deg) (4)	ϵ (5)	ϵ_{cor} (6)	$\mu(0)$ (7)	R_d (arcsec) (8)	R_{opt} (arcsec) (9)	$R_{23.5}$ (arcsec) (10)	$m_{23.5}$ (11)	m_∞ (12)	m_{cor} (13)	M_{cor} (14)	Notes (15)
280132.....	5	10	100	0.570	0.635 (13)	18.9	2.0	6.8	8.6	16.66	16.58	16.24	−20.71 (06)	
280133.....	4:	18	66	0.584	0.623 (18)	20.8	4.0	8.4	10.0	16.26	16.11	15.80	−21.15 (05)	
280136.....	4	24	17	0.568	0.631 (15)	18.4	2.4	9.0	11.1	15.99	15.90	15.55	−21.63 (06)	[a]
A3744:														
610196.....	5	26	70	0.791	0.816 (15)	20.4	7.9	24.9	25.1	15.59	15.45	14.74	−20.55 (13)	[a]
610198.....	6	22	26	0.770	0.816 (14)	20.4	4.2	12.1	12.1	17.20	17.00	16.47	−18.82 (12)	[a]
34131	4:	68	20	0.547	0.557 (21)	21.0	8.5	33.3	18.4	15.80	15.36	14.96	−20.21 (15)	[a]
34135	4	65	120	0.569	0.599 (24)	15.4	3.2	18.8	23.9	13.48	13.44	13.11	−22.07 (07)	
610212.....	5	60	102	0.816	0.857 (14)	18.9	3.7	13.2	15.5	16.47	16.38	15.57	−19.46 (13)	
610214.....	5	8	30	0.826	0.864 (08)	19.7	6.7	18.3	23.3	15.42	15.34	14.45	−20.84 (14)	
610217.....	4	52	98	0.696	0.731 (12)	20.6	5.5	14.1	14.8	16.19	16.01	15.43	−19.79 (11)	
610220.....	1	14	80	0.496	0.528 (19)	18.5	3.2	10.2	15.1	14.65	14.60	13.98	−21.31 (08)	[a]
610222.....	5	9	73	0.745	0.817 (30)	14.3	2.3	15.2	19.4	14.31	14.28	13.55	−21.74 (15)	[a]
610224.....	5	6	45	0.672	0.706 (15)	19.7	4.2	11.8	14.6	15.90	15.80	15.26	−20.03 (10)	
610231.....	3	50	27	0.470	0.490 (11)	19.5	4.9	14.6	18.1	14.72	14.61	14.26	−20.92 (07)	
34189	5	26	165	0.766	0.781 (16)	20.6	11.3	25.5	29.9	14.63	14.49	13.84	−20.81 (11)	[a]
610251.....	6	28	10	0.807	0.848 (10)	19.7	4.3	11.9	14.5	16.72	16.63	16.04	−18.63 (11)	[a]
A2457:														
320569.....	1	37	26	0.679	0.697 (18)	20.8	9.5	21.1	25.0	14.48	14.34	13.65	−22.59 (08)	
320572.....	5	19	79	0.810	0.846 (11)	18.5	5.7	18.0	26.2	14.63	14.58	13.71	−22.48 (15)	[a]
320573.....	4	19	14	0.544	0.595 (55)	18.4	2.3	7.9	10.2	15.19	15.15	14.81	−21.38 (06)	[a]
320574.....	5	32	161	0.753	0.807 (11)	19.5	3.6	10.6	14.4	15.93	15.84	15.16	−21.41 (12)	[a]
320575.....	4:	17	6	0.791	0.832 (07)	18.9	4.7	12.2	20.0	15.25	15.23	14.42	−21.78 (14)	
320576.....	4:	12	93	0.375	0.384 (92)	20.0	8.9	25.0	25.6	13.94	13.81	13.61	−22.59 (06)	[a]
320578.....	5	39	116	0.809	0.857 (09)	18.9	4.4	14.2	19.1	15.61	15.55	14.69	−21.52 (14)	
320579.....	4B	23	72	0.490	0.529 (54)	18.4	2.7	11.2	12.6	15.32	15.23	14.84	−21.35 (07)	[a]
320581.....	1	11	6	0.496	0.527 (10)	18.6	3.5	10.2	16.0	14.41	14.36	13.77	−22.43 (07)	[a]
320583.....	4:	7	10	0.682	0.728 (10)	18.8	3.4	10.4	14.9	15.36	15.31	14.83	−21.37 (09)	[a]
320591.....	5	19	92	0.819	0.856 (08)	18.6	5.8	19.6	25.8	14.96	14.90	14.04	−21.16 (14)	[a]

[a] See § 3 for notes on individual galaxies.

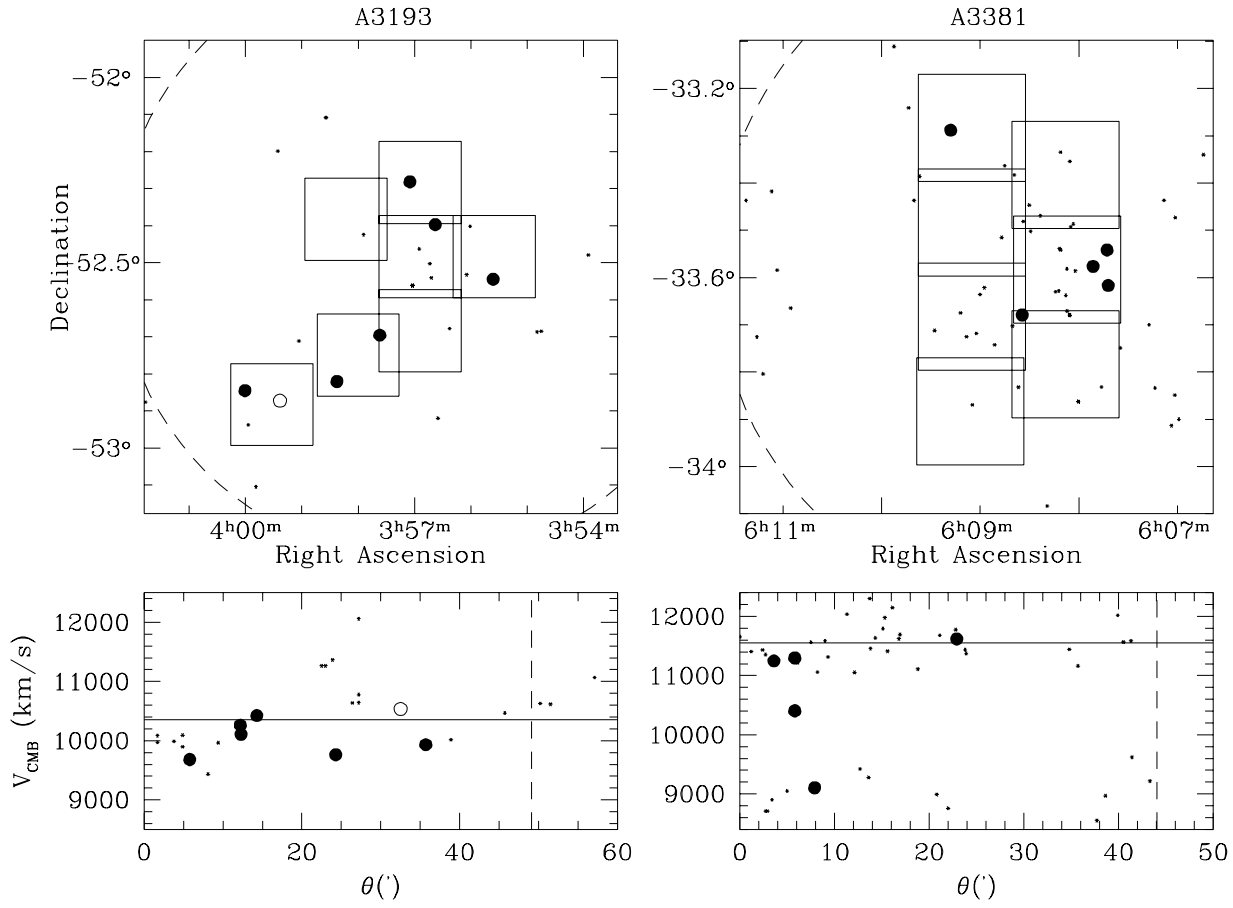

FIG. 4.—Same as Fig. 2, but for the clusters Abell 3193 and Abell 3381

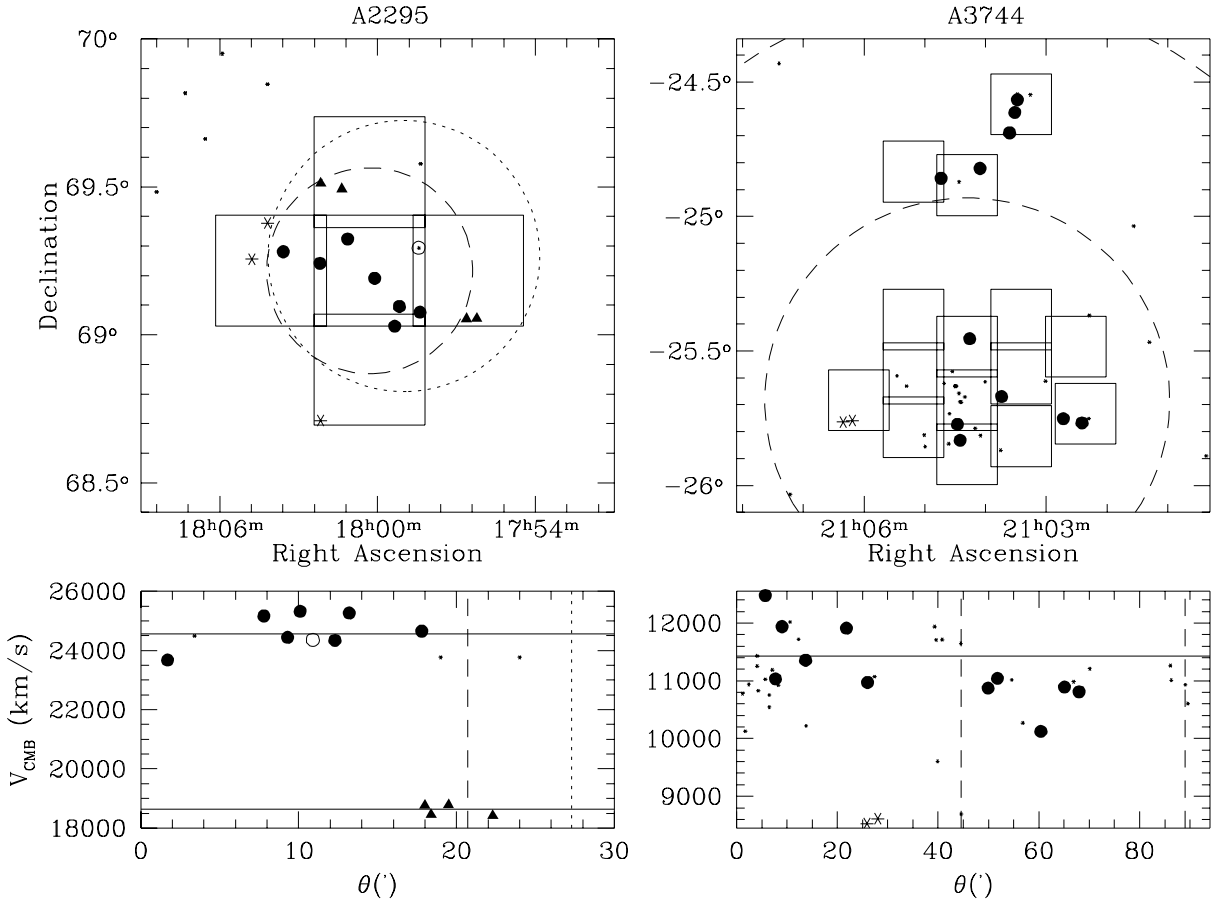

FIG. 5.—Same as Fig. 2, but for the clusters Abell 2295, Abell 2295B, and Abell 3744. For A2295B (*left*), filled triangles identify cluster members and $1R_A$ is indicated by the dotted line in the bottom panel and by the dotted circle of radius $1R_A$ in the top panel.

implies 13241 ± 08.

Column (*6*).—The raw velocity width in km s^{-1}. Measurement of optical widths are described in § 2.2; 21 cm line widths are indicated by footnotes and refer to values measured at a level of 50% of the profile horns.

Column (*7*).—The velocity width in km s^{-1} after correcting for ORC shape, the cosmological stretch of the data, and, for 21 cm data, signal-to-noise effects, interstellar medium turbulence, and instrumental and data-processing broadening; details on the adopted corrections for optical and 21 cm data are given in § 2.2 and G97a, respectively.

Column (*8*).—The corrected velocity width in km s^{-1} converted to an edge-on perspective.

Column (*9*).—The adopted inclination i of the plane of the disk to the line of sight, in degrees (90° corresponding to edge-on perspective); the derivation of i and its associated uncertainty are discussed in § 4 of Paper I.

Column (*10*).—The logarithm in base 10 of the corrected velocity width (value in col. [7]), together with its estimated uncertainty in parentheses. The uncertainty takes into account both measurement errors and uncertainties arising from the corrections. The format 2.576 (22), for example, is equivalent to 2.576 ± 0.022.

The position angle adopted for the slit of each spectroscopic observation is that given in column (4) of Table 3. The first column in Table 3 matches that of Table 2. The remaining listed parameters for Table 3 are as follows:

Column (*2*).—Morphological type code in the RC3 scheme, where code 1 corresponds to Sa's, code 3 to Sb's, code 5 to Sc's, and so on. When the type code is followed by a "B," the galaxy disk has an identifiable bar. We assign these codes after visually inspecting the CCD I-band images and after noting the value of R_{75}/R_{25}, where R_X is the radius containing X% of the I-band flux. This ratio is a measure of the central concentration of the flux that was computed for a variety of bulge-to-disk ratios. Given the limited resolution of the images, some of the inferred types are rather uncertain; these are followed by a colon.

Column (*3*).—The angular distance θ in arcminutes from the center of each cluster.

Column (*4*).—Position angle of the major axis of the image, also used for spectrograph slit positioning (north: 0°; east: 90°).

Column (*5*).—Observed ellipticity of the disk.

Column (*6*).—Ellipticity corrected for seeing effects as described in § 5 of Paper I, along with its corresponding uncertainty. The format 0.780 (16), for example, is equivalent to 0.780 ± 0.016.

Column (*7*).—Surface brightness of the disk at zero radius, as extrapolated from the fit to the disk surface brightness profile.

Column (*8*).—The (exponential) disk scale length.

Column (*9*).—The distance along the major axis to the isophote containing 83% of the I-band flux.

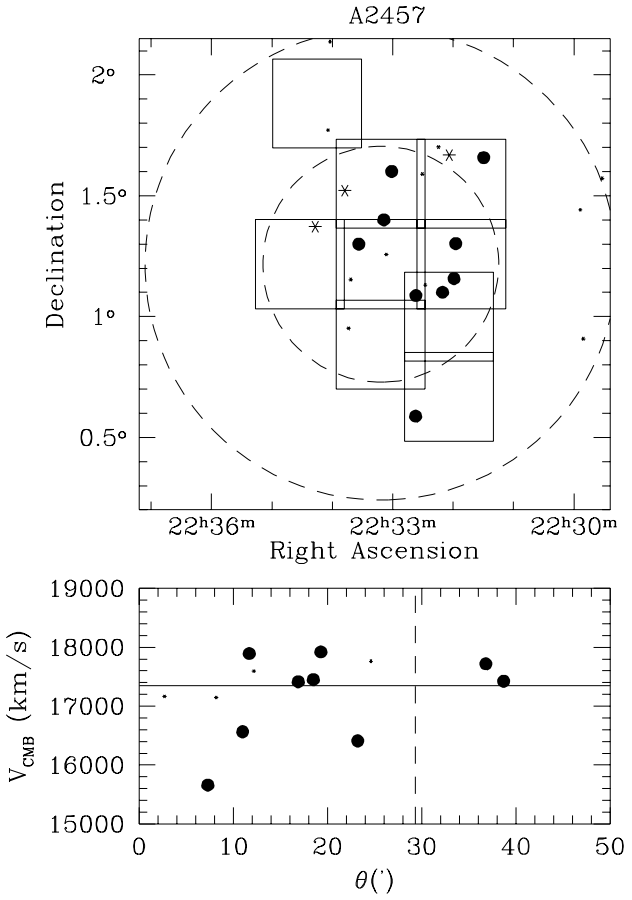

FIG. 6.—Same as Fig. 2, but for the cluster Abell 2457

Column (*10*).—Isophotal radius along the major axis where the surface brightness equals 23.5 mag arcsec^{-2}.

Column (*11*).—Apparent magnitude within the 23.5 mag arcsec^{-2} isophote.

Column (*12*).—The measured *I*-band magnitude, extrapolated to infinity assuming that the surface brightness profile of the disk is well described by an exponential function.

Column (*13*).—The apparent magnitude, to which *k*-term and Galactic and internal extinction corrections were applied; details on the adopted corrections are given in § 2.1.

Column (*14*).—The absolute magnitude, computed assuming that the galaxy is at the distance indicated either by the cluster redshift, if the galaxy is a cluster member within $1R_A$ of the cluster center, or by the galaxy redshift if not. The calculation assumes $H_0 = 100\,h$ km s^{-1} Mpc^{-1}, so the value listed is strictly $M_{cor} - 5 \log h$. In calculating this parameter, radial velocities are expressed in the CMB frame and uncorrected for any cluster peculiar motion. The uncertainty, indicated in parentheses in hundredths of a magnitude, is the sum in quadrature of the measurement errors and the estimate of the uncertainty in the corrections applied to the measured parameter.

In both tables, when a footnote appears in the last column, a detailed comment is given for that particular object. Because of the length and number of these comments, they are not appended to the table but are included in the text as follows. Note that a galaxy is flagged in both Tables 2 and 3, independently of whether the comments refer only to the photometry, only to the spectroscopy, or to both.

A2806:
- 20391 Possible disk warp; [N II] patch for radii less than 8″.
- 400698 Mostly bulge ORC; uncertain extrapolation.
- 400703 Mostly bulge ORC; uncertain extrapolation. Unfit for T-F use.
- 400713 Mostly bulge ORC; large extrapolation; exponential disk over narrow range of radii.

A114:
- 400672 Exponential disk over narrow range of radii.
- 400443 Uncertain ellipticity; Hα absorption in bulge—[N II] patch for radii less than 3″; two nuclei?
- 400453 Uncertain position angle.

A119:
- 400619 Exponential disk over narrow range of radii; Hα absorption in bulge—[N II] patch for radii less than 2.″5.
- 400600 Uncertain ORC extrapolation; [N II] line used.
- 400641 Uncertain ellipticity; [N II] patch for radii $\lesssim$2″.
- 400658 Background galaxy.

A194:
- 784 Only 21 cm width available.
- 830 Only 21 cm width available; note low *i*. Unfit for T-F use.
- 894 Foreground galaxy; only 21 cm width available.
- 915 Background galaxy; only 21 cm width available.
- 931 Foreground galaxy; only 21 cm width available.
- 410584 Asymmetric nucleus.
- 1116 Only 21 cm width available.
- 1120 Only 21 cm width available.
- 1123 Only 21 cm width available.

A3193:
- 23113 Note low *i*.
- 23130 Extremely low surface brightness at radii $\gtrsim$20″; heavy Hα absorption throughout disk. Unfit for T-F use.
- 23136 Note low *i*; [N II] patch for radii $\lesssim$0.″5.

A3381:
- 460069 Rising ORC; uncertain extrapolation.
- 460071 Hα absorption in bulge.
- 24895 Companion galaxy 35″ to southeast.

A2295B:
- 270370 Rising ORC; uncertain extrapolation; uncertain position angle.
- 280128 Mostly bulge ORC.
- 280130 Star 40″ to west-northwest.
- 280134 Foreground galaxy.

A2295:
- 270375 Rising ORC; note low *i*; small companion galaxy 10″ to east. Unfit for T-F use; 5 minute integration.
- 280131 Background galaxy.
- 280136 Background galaxy.

A3744:
- 610196 Rising ORC; large extrapolation.
- 610198 Rising ORC.
- 34131 Faint disk; large extrapolation made to ORC.
- 610220 Heavy Hα absorption in one half of disk.
- 610222 Slightly rising ORC.
- 34189 Foreground galaxy; patchy H II distribution.

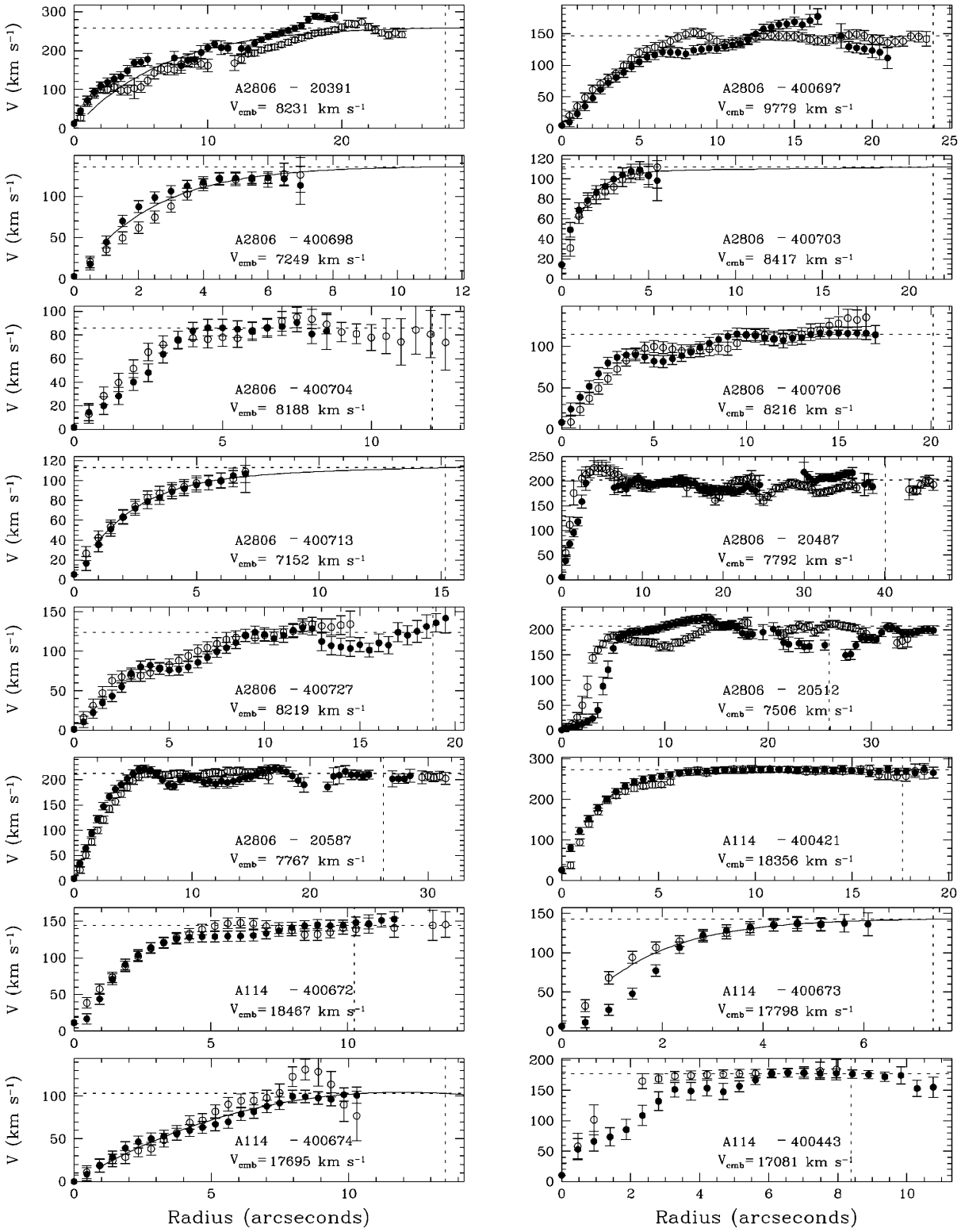

FIG. 7.—Hα rotation curves for 82 galaxies (except for galaxies 400600 and 320572, for which the ORCs are obtained from an [N II] emission line), folded about the kinematic centers. The error bars include both the uncertainty in the wavelength calibration and the ORC fitting routine used. Names of the galaxy and the corresponding parent cluster are given along with the CMB radial velocity. In each panel, two dashed lines are shown: the horizontal line indicates the adopted half-velocity width, $W/2$, which in some cases arises from an extrapolation to the ORC or from a 21 cm width (see Table 2); the vertical line is at R_{opt}, the radius containing 83% of the I-band flux. For those cases in which a shape correction to the velocity width was used, a fit to the ORC is indicated by a solid line. Note that the rotation curves are *not* deprojected to an edge-on orientation.

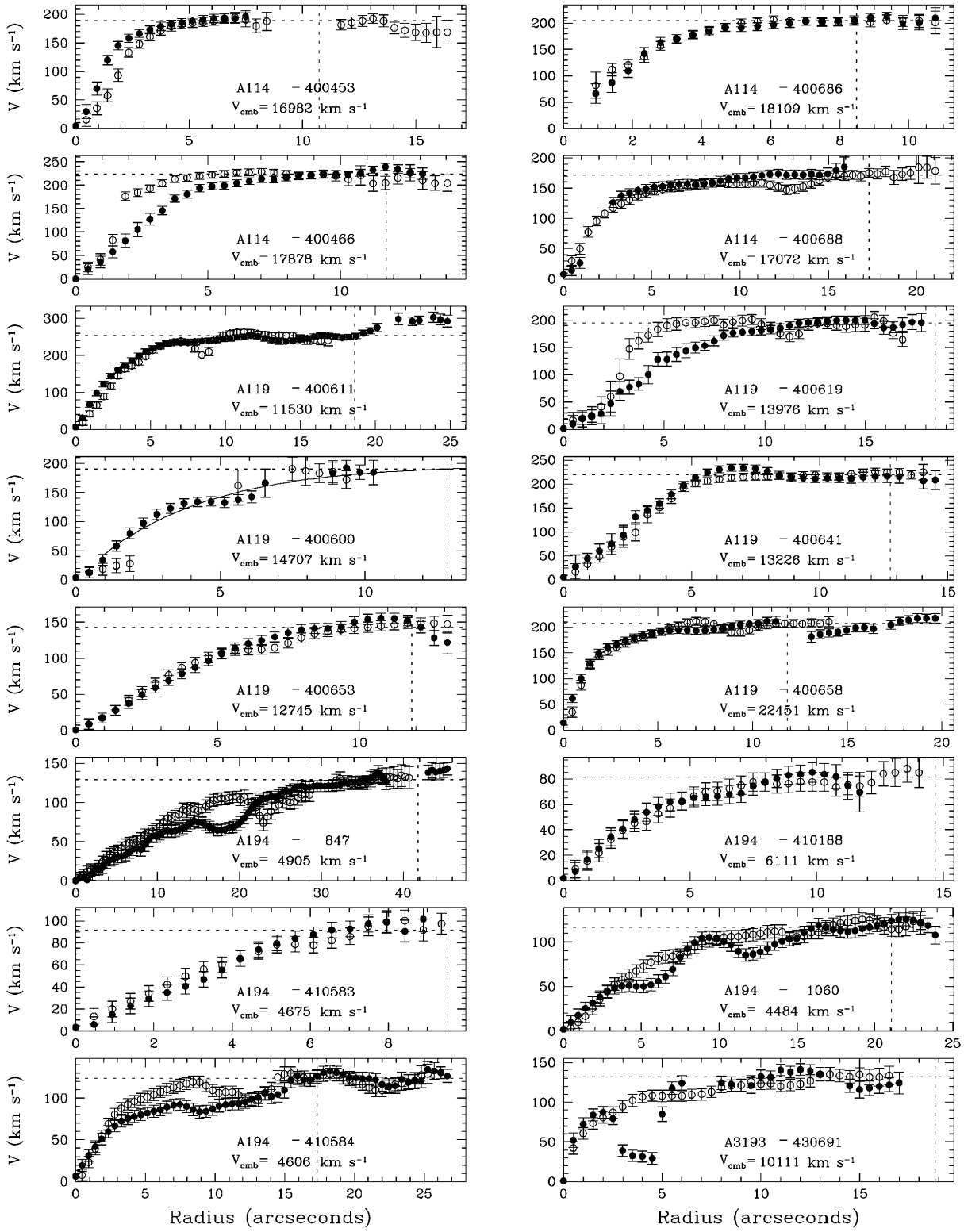

FIG. 7.—*Continued*

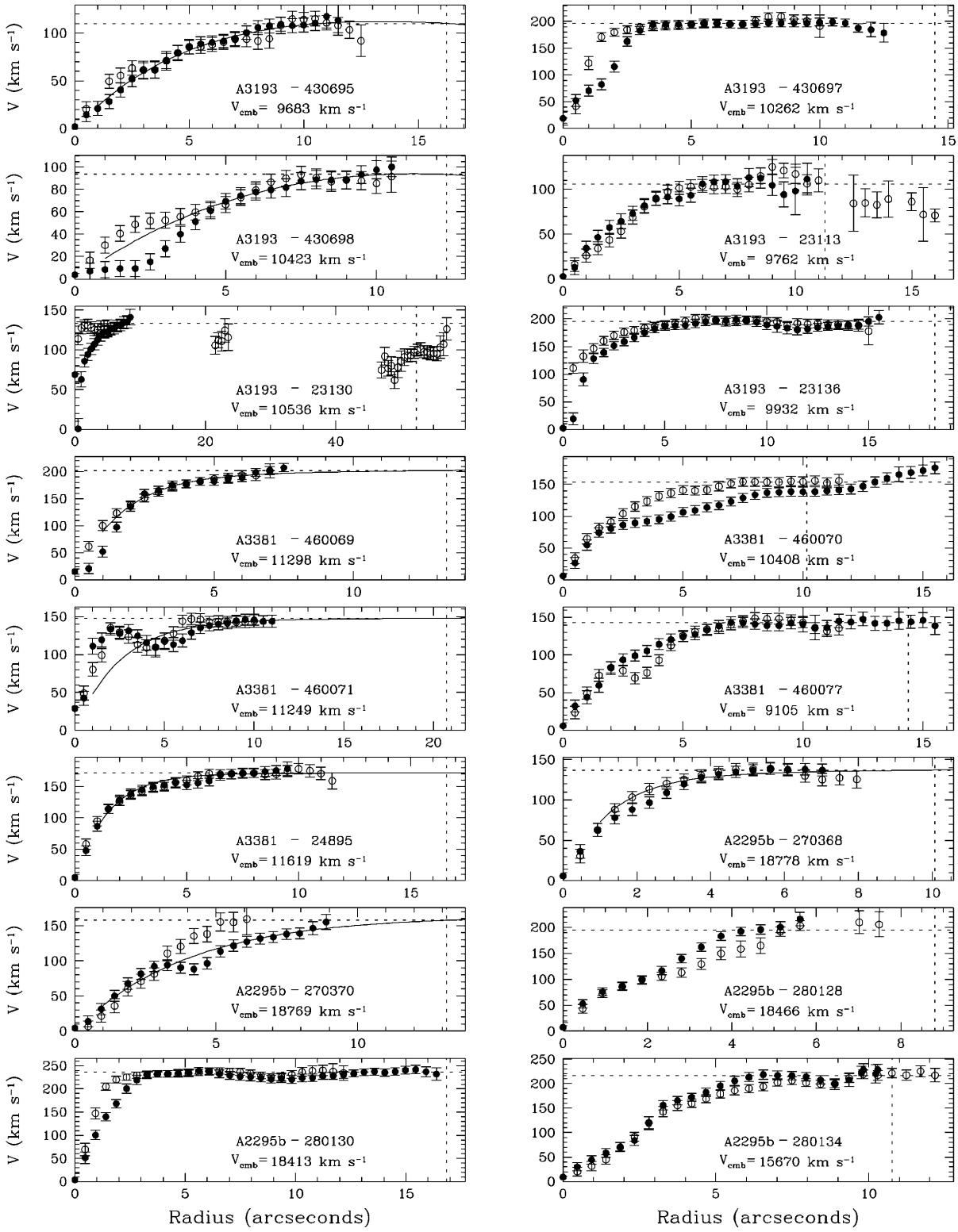

FIG. 7.—*Continued*

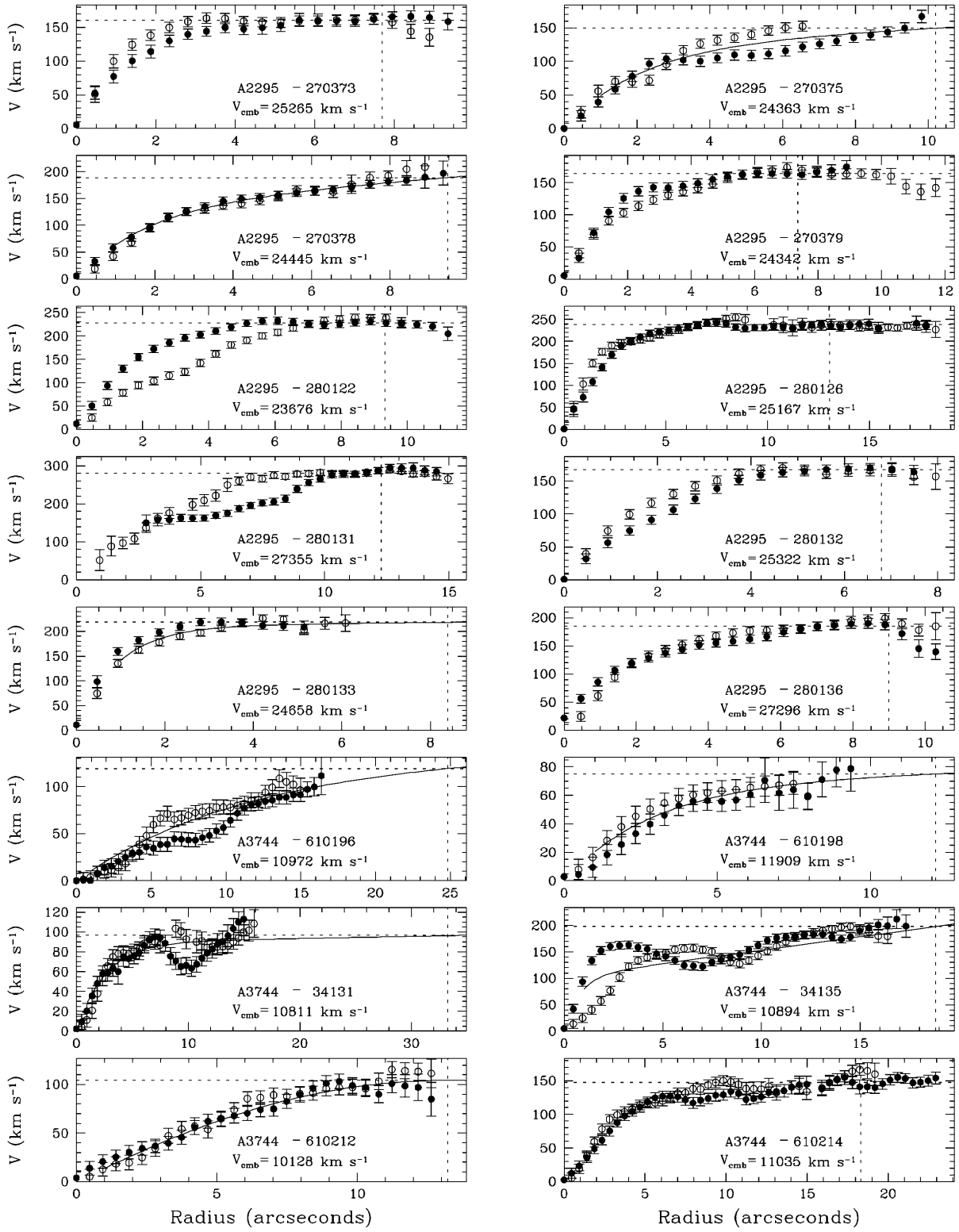

FIG. 7.—*Continued*

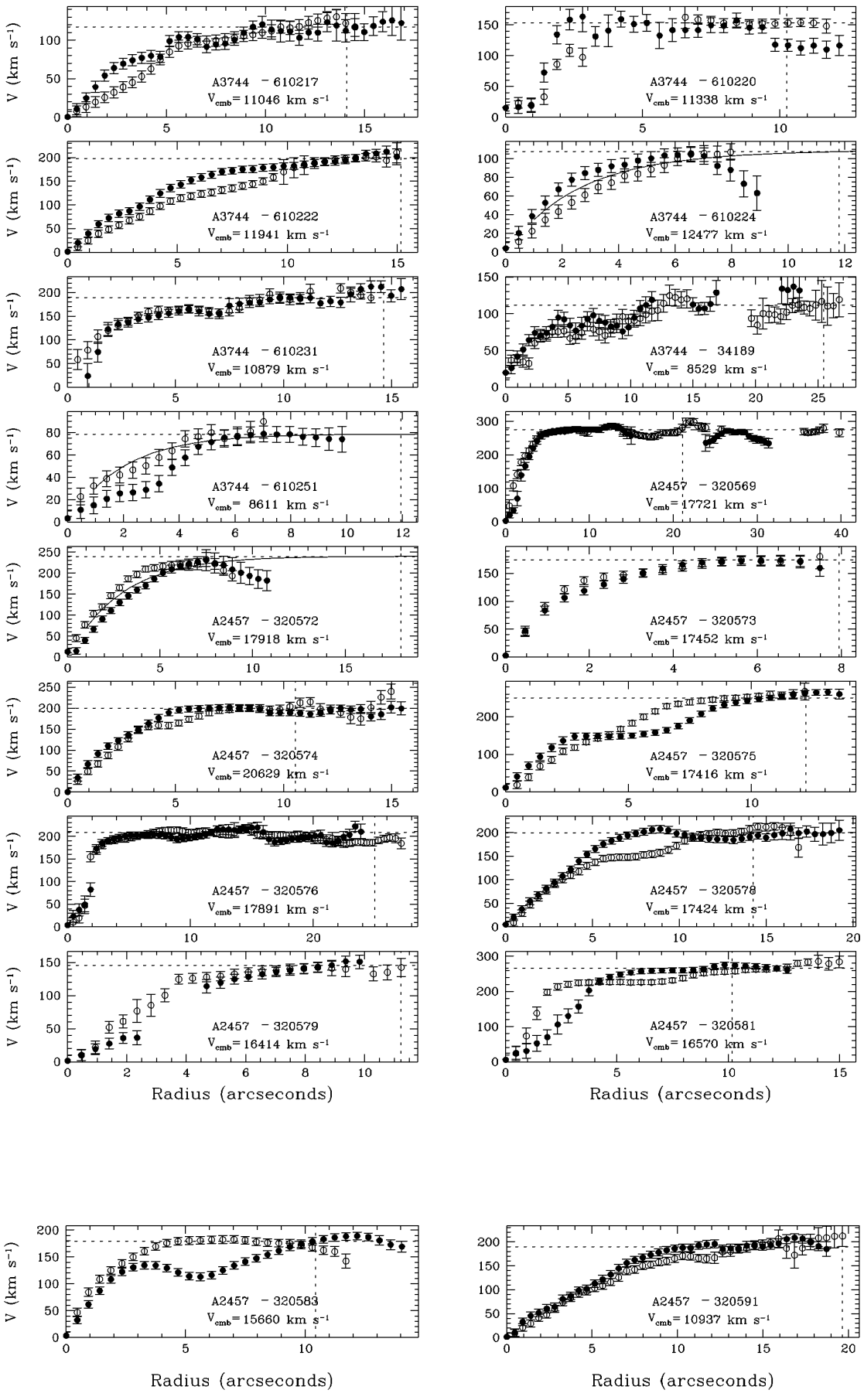

FIG. 7.—*Continued*

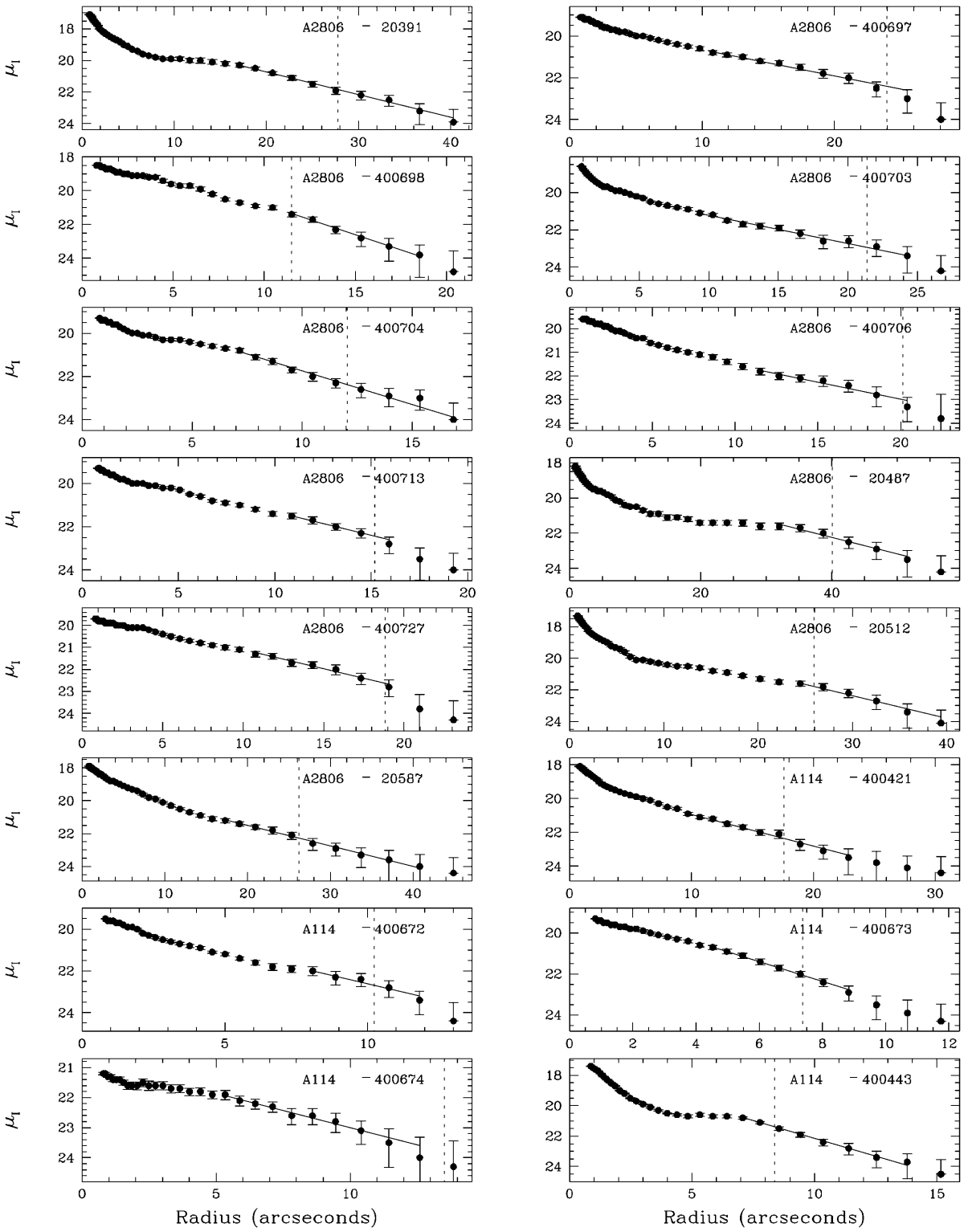

FIG. 8.—A sampling of surface brightness profiles. The name of the galaxy and the corresponding parent cluster are given in each panel. Two lines are drawn: the vertical dashed line is drawn at R_{opt} and the solid line is an exponential fit to the disk, over the range of radii over which the disk is assumed to behave exponentially.

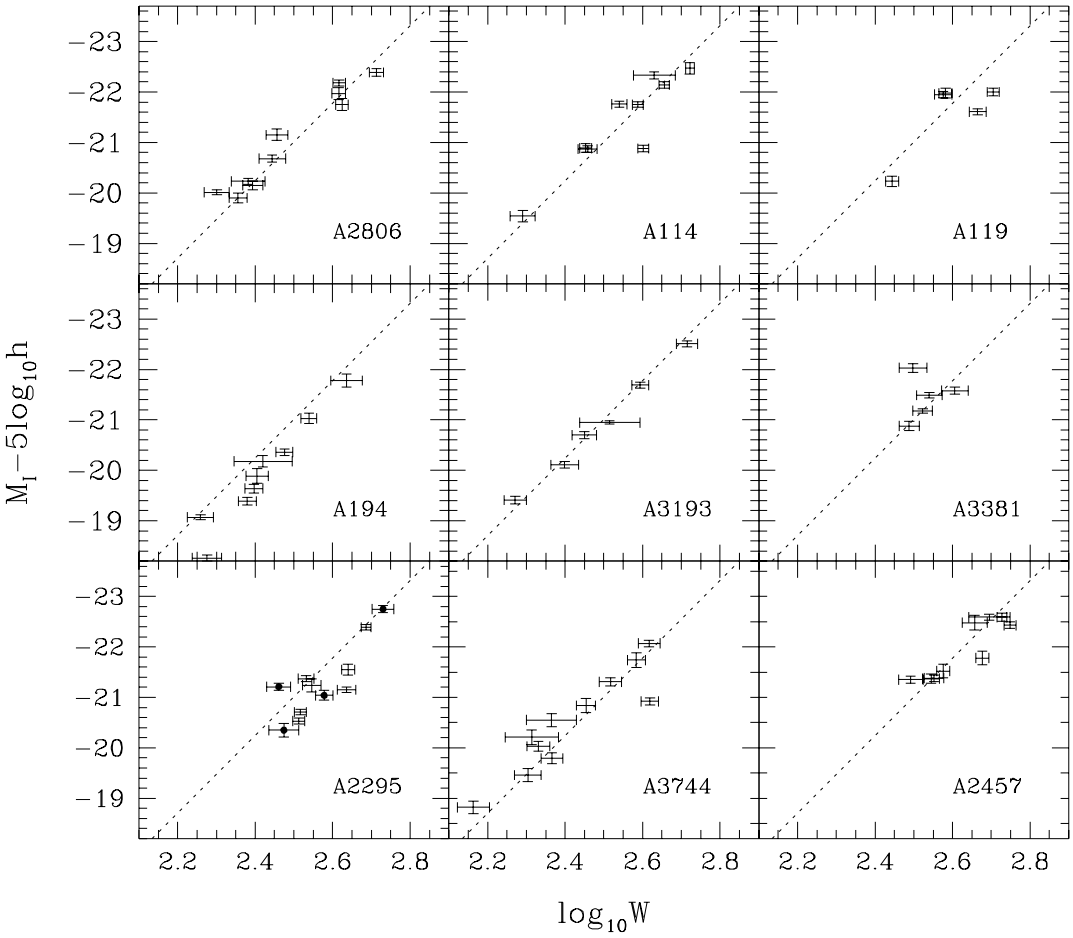

FIG. 9.—"Raw" T-F plots for the 10 clusters. We emphasize that the data have *not* been corrected for incompleteness bias. In the A2295 panel, the error bars containing filled circles represent members of "A2295B," a cluster at a lower redshift than A2295. The dashed line is the template relation valid for low-z clusters (eq. [4]).

610251 Foreground galaxy.

A2457:

320572 Mostly bulge ORC; large correction applied to W_{ORC}; [N II] line used.
320573 Outer isophotes differ in ellipticity and position angle with respect to inner isophotes.
320574 Backgroud galaxy.
320576 Star 55″ to northeast; uncertain ellipticity; [N II] patch for radii $\lesssim 1\farcs5$.
320579 Slightly rising ORC; uncertain ellipticity; [N II] patch for radii $\approx 2''$–$4''$.
320581 [N II] patch for radii $\lesssim 2''$.
320583 Asymmetric; merger?
320591 Foreground galaxy; 5 minute integration.

In Figure 7, we plot the ORCs folded about a kinematic center as described in § 2.2. The horizontal dashed line in each panel indicates the adopted (and uncorrected for inclination) half-velocity width, $W/2$, for each galaxy, and the vertical dashed line is drawn at R_{opt}. We have overlaid fits to the ORCs for the cases in which shape corrections to the velocity widths were necessary. Finally, in Figure 8 we show, as an example, the surface brightness profiles for the first 16 galaxies in Figure 7. Again the vertical dashed line refers to R_{opt}. The solid line drawn along the disk is the fit to the disk over the range of radii assumed to cover the exponential portion of the disk. The remainder of the plots of surface brightness profiles for the complete sample can be obtained by contacting D. A. D.

Figure 9 shows the "raw" T-F plots of each cluster, uncorrected for any incompleteness bias. A computation of such bias will be presented in future work when data from all clusters is in hand. Furthermore, the cluster systemic redshifts used in obtaining these plots are preliminary. Included in the T-F plots is the template relation obtained from nearby clusters in G97b:

$$y = -7.68x - 21.01\ , \qquad (4)$$

where $y = M_{cor} - 5\log h$ and $x = \log W_{cor} - 2.5$.

We thank Katie Jore for the use of her ORC fitting programs. The results presented here are based on observations carried out at the Palomar Observatory, Kitt Peak National Observatory, Cerro Tololo Inter-American Observatory, the (late) 300 foot telescope of the National Radio Astronomy Observatory (NRAO), and Arecibo Observatory, which is part of the National Astronomy and Ionosphere Center (NAIC). KPNO and CTIO are operated by the Association of Universities for Research in Astronomy, Inc., and NAIC is operated by Cornell University, all under cooperative agreements with the National Science Founda-

tion. The Hale Telescope at Palomar Observatory is operated by the California Institute of Technology under a cooperative agreement with Cornell University and the Jet Propulsion Laboratory. NRAO is operated by Associated Universities, Inc., under a management agreement with NSF. This research was supported by NSF grants AST 94-20505 to R. G. and AST 95-28960 to M. P. H.; L. E. C. was partially supported by FONDECYT grant 1970735.

REFERENCES

Abell, G., Corwin, H. G., & Olowin, R. P. 1989, ApJS, 70, 1
Branchini, E., Plionis, M., & Sciama, D. W. 1996, ApJ, 461, L17
Burstein, D., & Heiles, C. 1978, ApJ, 225, 40
Courteau, S., Faber, S., Dressler, A., & Willick, J. 1993, ApJ, 412, L51
Dale, D., Giovanelli, R., Haynes, M., Scodeggio, M., Hardy, E., & Campusano, L. 1997, AJ, 114, 455 (Paper I)
de Vaucouleurs, G., de Vaucouleurs, A., Corwin, H. G., Jr., Buta, R. J., Paturel, G., & Fouqué, P. 1991, Third Reference Catalogue of Bright Galaxies (New York: Springer)
Giovanelli, R., Haynes, M. P., Dale, D. A., & Hardy, E. 1998, in preparation
Giovanelli, R., Haynes, M. P., Herter, T., Vogt, N. P., Wegner, G., Salzer, J. J., da Costa, L. N., & Freudling, W. 1997a, AJ, 113, 22 (G97a)
Giovanelli, R., Haynes, M. P., Herter, T., Vogt, N. P., da Costa, L. N., Freudling, W., Salzer, J. J., & Wegner, G. 1997b, AJ, 113, 53 (G97b)
Giovanelli, R., Haynes, M. P., Wegner, G., da Costa, L. N., Freudling, W., & Salzer, J. J. 1996, ApJ 464, L99
Han, M. 1992, ApJS, 81, 35
Haynes, M. P., & Giovanelli, R. 1991, ApJS, 77, 331
Haynes, M. P., Giovanelli, R., Salzer, J. J., Wegner, G., Freudling, W., da Costa, L. N., Herter, T., & Vogt, N. P. 1998, in preparation
Kogut, A., et al. 1993, ApJ, 419, 1
Lauer, T., & Postman, M. 1994, ApJ, 425, 418 (LP)
Persic, M., & Salucci, M. 1991, ApJ, 368, 60
———. 1995, ApJS, 99, 501
Riess, A., Press, W., & Kirshner, R. 1995, ApJ, 445, L91
Scaramella, R., Vettolani, G., & Zamorani, G. 1994, ApJ, 422, 1
Tini-Brunozzi, P., Borgani, S., Plionis, M., Moscardini, L., & Coles, P. 1995, MNRAS, 277, 1210
Tully, R. B., & Fisher, J. R. 1977, A&A, 54, 661
Watkins, R., & Feldman, H. 1995, ApJ, 453, L73